International Journal of Fluid Machinery and Systems
Vol. 1, No. 1, October-December 2008

Original Paper

Unsteady Flows Arising in a Mixed-Flow Vaneless Diffuser System

Hiromu Tsurusaki

Department of Mechanical Systems Engineering, Fukuyama University
Fukuyama, Hiroshima 729-0292, Japan

Abstract

The main objective of this study was to clarify the origin of the unsteady flows arising in a mixed-flow vaneless diffuser system and also the effects of physical components of the system. The testing equipment consists of a straight tube, a swirl generator, and a mixed-flow vaneless diffuser. Pressure fluctuations of the flow through the tube and diffuser were measured by using a semiconductor-type pressure transducer and analyzed by an FFT analyzer. In the experiment, the velocity ratio (axial velocity/peripheral velocity) of the internal flow, and the geometric parameters of the diffuser were varied. Two kinds of unsteady flows were measured according to the combination of the components, and the origin of each unsteady flow was clarified. The fundamental frequencies of unsteady flows arose were examined by two-dimensional small perturbation analysis.

Keywords: Unsteady flow, Mixed-flow, Vaneless diffuser, Swirling flow, Pressure fluctuation, Rotating stall.

1. Introduction

Swirling flows exist in various kinds of flow equipments, for instance, in a vortex tube used as a spot cooling device, a swirl burner containing combustion gas having swirl velocity, an annular channel serving as a collector connected with the final stage of a multistage axial compressor (Escudier [1]), a draft tube of a water turbine, and a vaneless diffuser of mixed flow/radial flow turbomachinery. In these flow-channels, various types of unsteady flow are generated. A swirling vortex is necessary in the vortex tube of the spot cooling system (Kurosaka [2]). Rotating stall often occurs in a radial vaneless diffuser (Tsurusaki [3]), and spiral vortex (Nishi et al. [4], Cassidy and Falvey [5]) often occurs in a draft tube of a water turbine, and these phenomena limit the stable operation range of the machinery. Extensive research has been conducted on these harmful unsteady flows. However, studies on unsteady flow arising in the mixed-flow vaneless diffuser and inlet tube system are insufficient.

This paper describes the experimental and theoretical results for unsteady flows in the mixed-flow vaneless diffuser system. An experimental rig consisting of a straight tube, a swirl generator, and a mixed-flow vaneless diffuser was used. The rig is similar to Ranque-Hilsch tube (Kurosaka [2]). The effects of parameters such as diffuser width, diffuser diameter, and cone angle of the diffuser on rotational speed of the cell in unsteady flow were examined. On the basis of the findings, an empirical equation for rotational speed of the cell (low-speed mode) arising at the diffuser is proposed. The nondimensional rotational speeds of the cell were also examined by two-dimensional small perturbation analysis.

The results of this study are useful for understanding and also controlling unsteady flow arising in the mixed-flow vaneless diffuser system and various kinds of equipments containing swirl flow.

2. Experimental Apparatus

Figure 1 shows the experimental apparatus used in this study. The working fluid is air. Air pressurized in the blower is piped into the swirl generator, and introduced into the straight tube (flow rate Q_0). By extracting the portion of the inflow from the end plate (flow rate Q_1), flow rate through the diffuser Q (= Q_0-Q_1) is controlled. Space-averaged axial velocity, v, in front of the diffuser is obtained from $v = Q/\pi r_s^2$. Peripheral velocity, u, of the inflow (eight jets) at $r = r_s$ is obtained from $u = (4Q_0/8\pi d_j^2)\cos\theta$, where d_j = diameter of the jet-flow channel of the swirl generator (d_j = 8.6 mm) and θ = jet-flow angle from the tangent (θ = 30º).

Two kinds of diffusers, with cone angles α = 45º and 22.5º, were used. Table 1 shows the specifications of tested diffusers. The three kinds of diffusers, having hub radius ratios r_h/r_s =3.25, 2.44, and 1.63, were used for the casing in which r_e/r_s =3.25. The α = 22.5º diffuser has a casing radius ratio and a hub radius ratio both equal to 2.20. The width of the diffuser, b, is changed by axial movement of the hub. The radius of the diffuser, r_2, is defined as shown in Fig. 1. In the case where α = 45º and r_h/r_s = 3.25, and in the case where α = 22.5º and r_h/r_s = 2.20, the radius r_2 is changed according to the variation of width b. In the case where α =45º and r_h/r_s = 2.44 or 1.63, r_2 is equal to r_h. The straight tube with length ratios l/r_s = 5 is used.

Received June 10, 2008; revised October 22, 2008; accepted for publication October 23, 2008: Review conducted by Prof. Gu Chuangang. (Paper number O08003)
Corresponding author: Hiromu Tsurusaki, Professor, htsu@fume.fukuyama-u.ac.jp

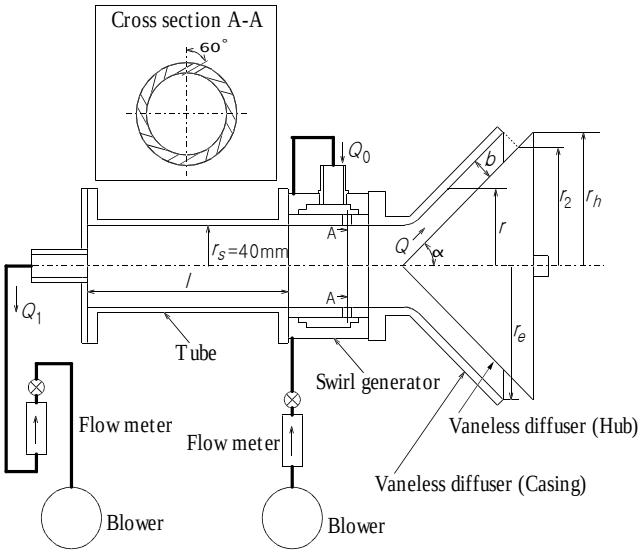

Fig. 1 Experimental apparatus.

Table 1 Specifications of diffusers.

α = 45 º	r_e/r_s =3.25	
	r_h/r_s	r_2/r_s
	3.25	Varied according to "b".
	2.44	2.44
	1.63	1.63
α = 22.5 º	r_e/r_s =2.20	
	r_h/r_s	r_2/r_s
	2.20	Varied according to "b".

3. Measurement Method

Pressure fluctuations were measured on the casing at the point r/r_s = 1.61 (r = radius at inner surface) for the α = 45º diffuser, and at r/r_s = 1.31 for the α = 22.5º diffuser, by using a semiconductor-type pressure transducer. Figure 2 depicts the measurement system. The frequency spectra of pressure fluctuations were measured by an FFT analyzer. A frequency spectrum was obtained from the ensemble average of 128 spectra by use of an averaging function of the FFT analyzer. The phase difference δ (degree) of the pressure fluctuations (fundamental components) between 2 points located γ (degree) apart on the circle (r/r_s = 1.26 for α = 45º, r/r_s = 1.50 for α =22.5º) was measured by the FFT analyzer. The number of cells, λ, of the unsteady flow was determined from $\lambda = \delta/\gamma$. The rotational speed of the cell, f_r, for unsteady flow of the fundamental frequency, f, was obtained from $f_r = f/\lambda$.

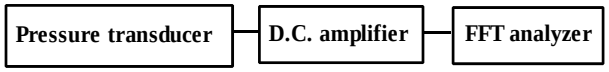

Fig. 2 Measurement system of pressure fluctuation.

4. Experimental Results and Discussion

4.1 Pressure Fluctuations due to Unsteady Flows

Figure 3 shows the frequency spectra of the pressure fluctuation measured for the rig with diffuser in which α = 45º, b = 20 mm. The peripheral velocity of the inflow is u = 9.3 m/s (Q_0 = 300 l/min). The space-averaged axial velocity was varied from v = 0.17 m/s (Q = 50 l/min) to v = 0.50 m/s (Q = 150 l/min). Unsteady flows having a fundamental frequency of about 3 Hz were generated. The measured number of cells was 1. For all unsteady flows measured in the present experiment, the number of cells was 1.

Figure 4(a) shows the variation of rotational speed of cell, f_r, with "u" and "v". However, by making "f_r" and "v" dimensionless, as shown in Fig. 4(b), the universal expression is obtained. It is same for pressure amplitude of the fundamental-frequency component (Tsurusaki and Yokota [6]). The velocity ratio, v/u, is a representative value for the flow angle at the section in front of the diffuser.

Figure 5 shows the relationship between nondimensional rotational speed of the cell, $\pi d_s f_r/u$, and the velocity ratio (tangent of the flow angle), v/u, for the rig with diffuser in which α = 45º, r_h/r_s = 3.25. In the present experiment, the critical value of v/u for the onset of the unsteady flow is about 0.1. Near v/u = 0, the nondimensional rotational speed is large when b/r_s is small.

Nondimensional rotational speed assumes a maximum value near $v/u = 0$.

Figure 6 shows the relationship between nondimensional pressure amplitude, $p/\rho u^2$, and v/u. The nondimensional pressure amplitude is large when b/r_s is small. A relatively strong fluctuation was measured near $v/u = 0$. The maximum value reaches about 10 % of ρu^2.

Figure 7 shows the measured result for the diffuser with small radius ($\alpha = 45^o$, $r_h/r_s = 1.63$). New unsteady flow was measured with nondimensional rotational speed 0.7 ~ 1.2, number of cells 1. This unsteady flow is called a high-speed mode, in contrast to the above-mentioned unsteady flow (low-speed mode).

For the diffuser in which $\alpha = 22.5^o$, as shown in Fig. 8, the low-speed mode appeared when $b/r_s \leq 0.5$, and the high-speed mode appeared when $b/r_s \geq 0.5$. Both modes appeared when $b/r_s = 0.5$ and $v/u = 0 \sim 0.04$. Although no figure is presented, the pressure amplitude of the high-speed mode is smaller than that of the low-speed mode.

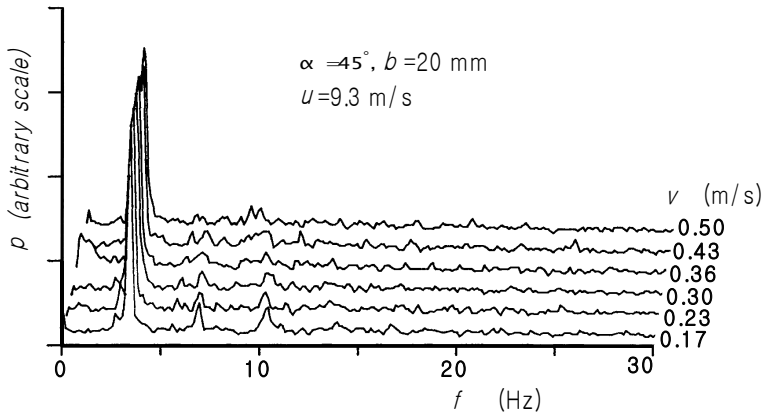

Fig. 3 Frequency spectra of pressure fluctuations.

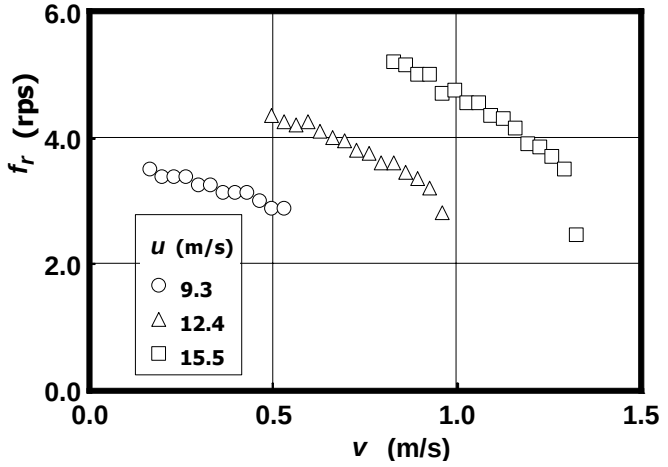

Fig. 4(a) Rotational speed of cell (α=45°, b=20mm, r_h/r_s=3.25, l/r_s=5).

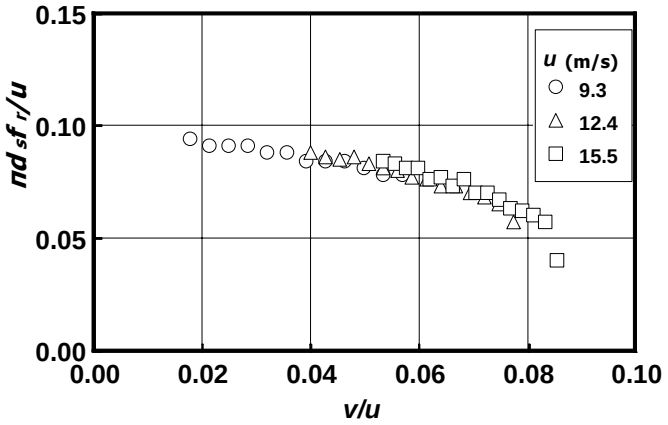

Fig. 4(b) Nondimensional rotational speed of cell (α=45°, b=20mm, r_h/r_s=3.25, l/r_s=5).

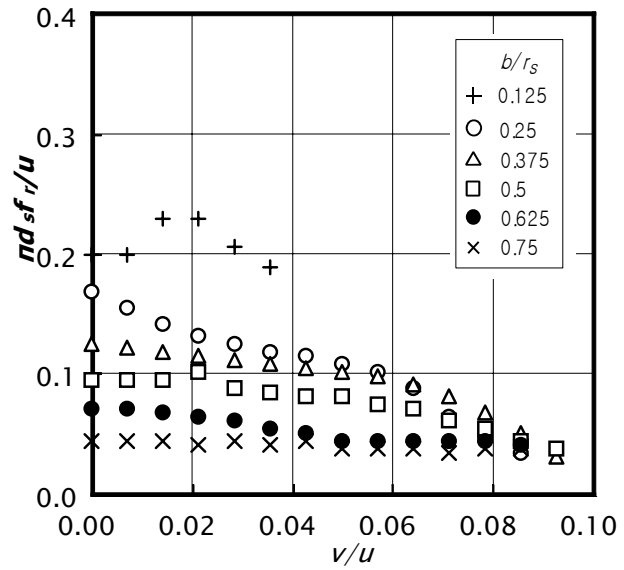

Fig. 5 Nondimensional rotational speed of cell (α=45°, r_h/r_s=3.25, l/r_s=5).

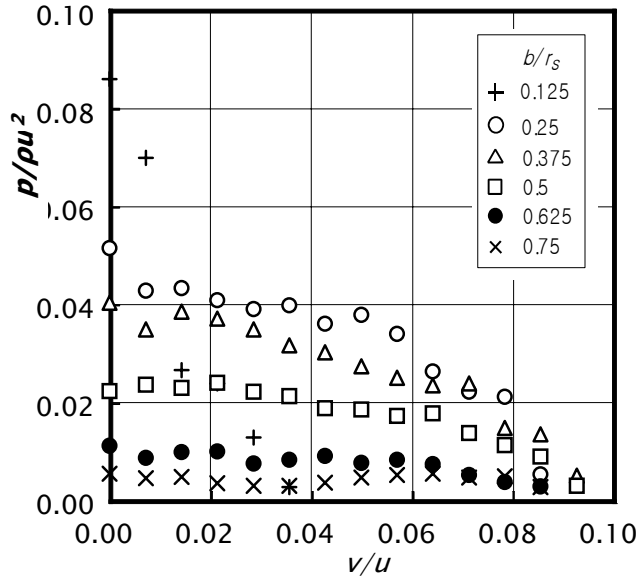

Fig. 6 Nondimensional pressure amplitude (α=45°, r_h/r_s=3.25, l/r_s=5).

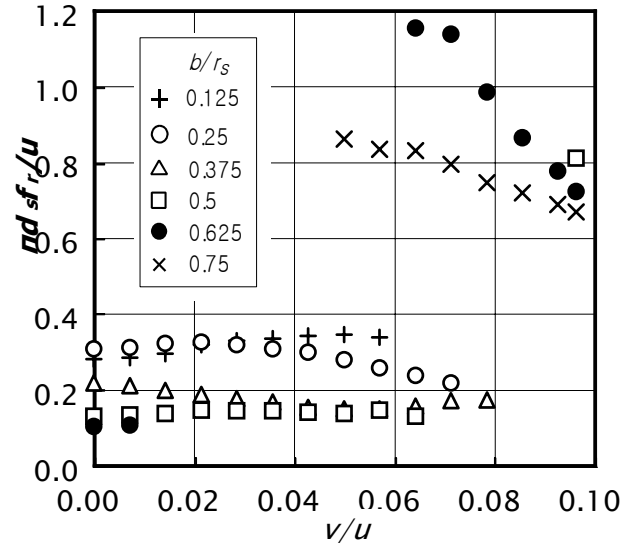

Fig. 7 Nondimensional rotational speed of cell (α=45°, r_h/r_s=1.63, l/r_s=5).

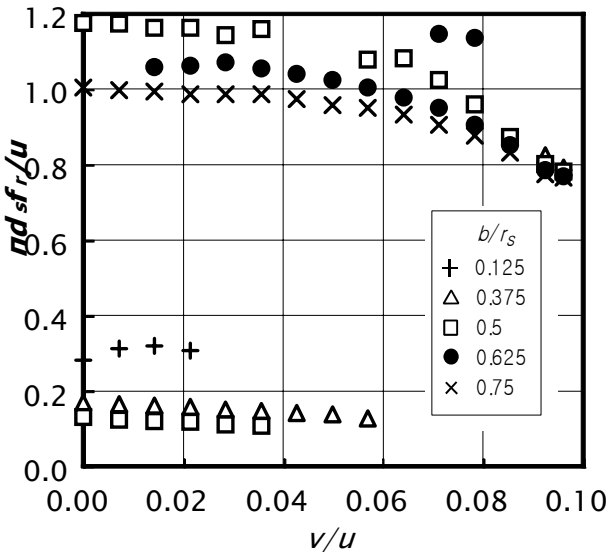

Fig. 8 Nondimensional rotational speed of cell (α=22.5º, r_h/r_s=2.20, l/r_s=5).

4.2 Origin of Unsteady Flows

Figures 9(a) and 9(b) show the frequency spectra measured at the casing wall and at the tube wall for the rig in which α = 22.5º, b/r_s = 0.5. The low-speed mode was not detected at the tube. Although no figure is presented, the low-speed mode was also generated for the rig in which α = 45º, l/r_s = 0 (without tube). From these experimental results, it is proven that the diffuser is the origin of the unsteady flow of low-speed mode.

As discussed in the later article 4.4.1, the low-speed mode can be explained as the instability of potential flow through the diffuser.

Figure 10 shows the frequency spectra measured at the casing wall in the case of the diffuser in which α = 22.5º and no tube is provided. The high-speed mode was not detected. From this experiment, it is believed that the origin of the high-speed mode is the tube, and the high-speed mode is due to the instability of combined vortex flow. It is discussed in the later article 4.4.2.

The present unsteady flow (high-speed mode) will be different from that observed in an open-end tube (Cassidy and Falvey [5]), because the diffuser in the test rig seriously affects the fundamental frequency and pressure amplitude.

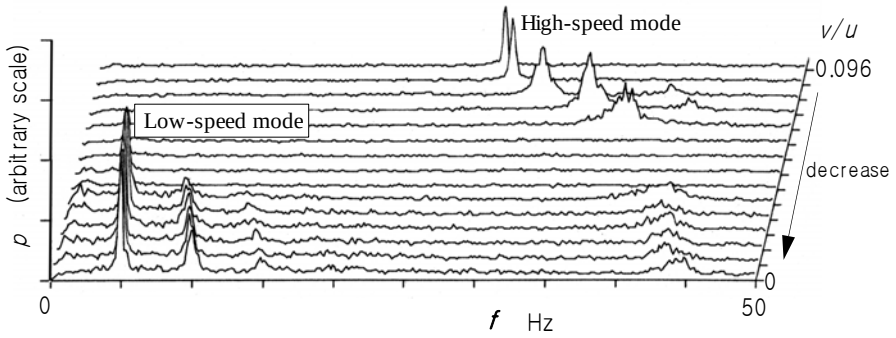

Fig. 9(a) Frequency spectra of pressure fluctuations measured at casing wall (α=22.5º, b/r_s=0.5, l/r_s=5).

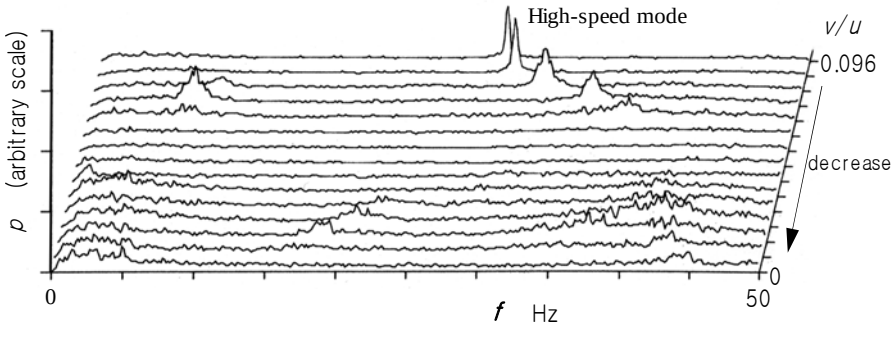

Fig. 9(b) Frequency spectra of pressure fluctuations measured at tube wall (α=22.5º, b/r_s=0.5, l/r_s=5).

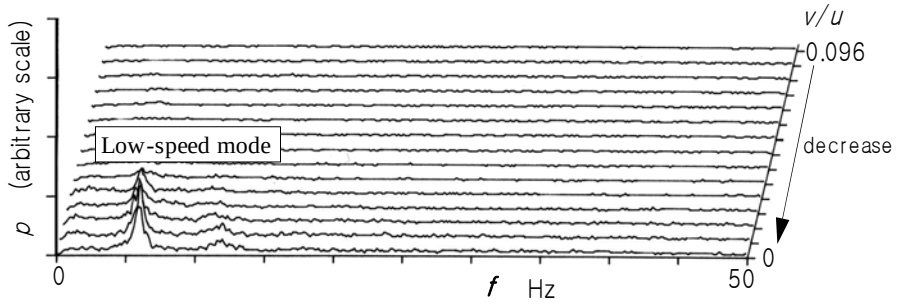

Fig. 10 Frequency spectra of pressure fluctuations measured at casing wall (α=22.5º, b/r_s=0.5, l/r_s=0).

4.3 Effect of Geometric Parameters of Diffuser

Figure 11 shows the relationship between radius ratio r_2/r_s of the diffuser and nondimensional rotational speed at v/u = 0 for the rig with the diffuser in which α = 45º, r_h/r_s =3.25, 2.44, and 1.63. Nondimensional rotational speed decreases as r_2/r_s is increased. This characteristic is well known for rotating stall of radial vaneless diffusers.

From curve fitting of measured nondimensional rotational speeds (low-speed mode), equation (1) was derived as a function of b/r_2 and r_2/r_s. The application range of the equation is r_2/r_s = 1.6 ~ 3.2 and b/r_2 = 0.04 ~ 0.38. The solid lines shown in Fig. 11 are based on equation (1).

$$\frac{\pi d_s f_r}{u} = -0.692(b / r_2) - 0.117(r_2 / r_s) + 0.558 \tag{1}$$

Figure 12 compares the predicted values based on equation (1) and the measured values for the rigs with diffusers in which α = 45º and α = 22.5º. This figure confirms that equation (1) is applicable to diffusers in which α = 45º and α = 22.5º. And also, it is expected that equation (1) is applicable to the diffusers in a range between α = 45º and α = 22.5º.

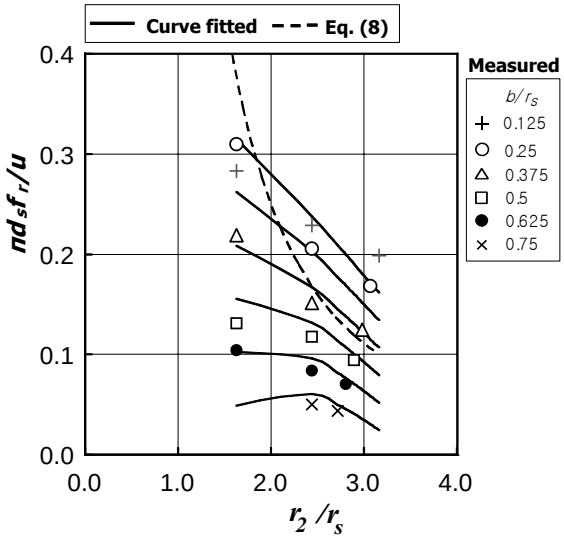

Fig. 11 Effect of diffuser radius (α=45º, l/r_s=5, v/u=0).

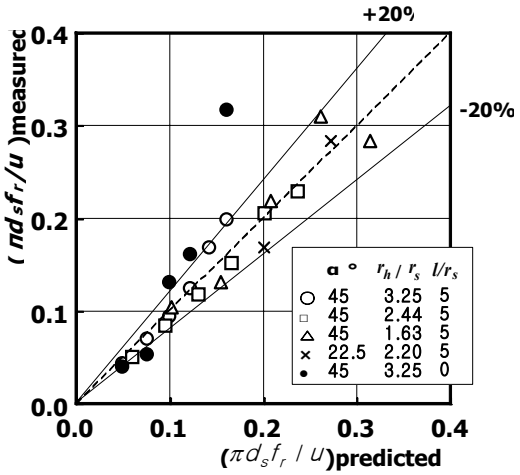

Fig. 12 Comparison of predicted and measured values (v/u=0).

4.4 Theoretical Consideration on Rotational Speeds of Cell

4.4.1 Instability of Flow in Mixed-Flow Diffuser (Low-Speed Mode)

It is expected that the low-speed mode is due to instability of the flow in the diffuser. This is examined by two-dimensional small perturbation analysis.

As shown in Fig. 13, an axisymmetric model of the diffuser is considered. On the basis of the discussion (Tsurusaki and Yokota [6]) on the causal relation between the generation of unsteady flow and the development of a back flow layer on the hub, a conical flow plane O-E is considered on the hub. The fluid is assumed to be inviscid and incompressible. Two-dimensional flow is expressed by coordinates s (O-E direction) and θ (peripheral direction). The origin of s is on the vertex of the hub. The flow rate is assumed to be zero. As shown in the following equation, velocity components and pressure are each expressed as the sum of a steady component and a small perturbation component, where ω is angular velocity and i is imaginary unit.

$$v_s = \tilde{v}_s(s)e^{i(\lambda\theta-\omega t)} \tag{2}$$

$$v_\theta = v_0(s) + \tilde{v}_\theta(s)e^{i(\lambda\theta-\omega t)} \tag{3}$$

$$p = p_0(s) + \tilde{p}(s)e^{i(\lambda\theta-\omega t)} \tag{4}$$

Linearized equations of motion are expressed as follows.

$$\frac{d\tilde{v}_s}{ds} + \frac{\tilde{v}_s}{r}\sin\alpha + \frac{i\lambda}{r}\tilde{v}_\theta = 0 \tag{5}$$

$$i(-\omega + \frac{\lambda v_0}{r})\tilde{v}_s - \frac{2v_0\tilde{v}_\theta}{r}\sin\alpha = -\frac{1}{\rho}\frac{d\tilde{p}}{ds} \tag{6}$$

$$i(-\omega + \frac{\lambda v_0}{r})\tilde{v}_\theta + (\frac{dv_0}{ds} + \frac{v_0}{r}\sin\alpha)\tilde{v}_s = -\frac{i\lambda}{\rho r}\tilde{p} \tag{7}$$

For time-averaged flow, forced vortex motion ($v_0 = r\Omega$) at $0 \le s \le s_1$ and free vortex motion ($rv_0 = K$) at $s_1 \le s \le s_2$ are assumed. The velocity components and pressures in two regions are continuous at $s = s_1$, respectively. Assumed boundary conditions are that perturbation of v_s is zero at s= 0, and perturbation of p is zero at $s = s_2$. Upon solving equations (5)-(7), two angular velocities (eigenvalues) are obtained. From these angular velocities, nondimensional rotational speeds are obtained as shown in the following equations, where $r_s u = r_2 v_0(s_2)$, circulation is constant, is assumed.

$$(\pi d_s f_r / u)_1 = (r_s / r_2)^2 \tag{8}$$

$$(\pi d_s f_r / u)_2 = (r_s / r_1)^2\left[1 - \{1 + (r_1 / r_2)^{2\lambda/\sin\alpha}\}(\sin\alpha / \lambda)\right] \tag{9}$$

Equation (8) is obtained by assuming free vortex motion on the flow plane O-E. The broken line in Fig. 11 shows the theoretical value by equation (8). Although the theoretical and measured values are not similar, the order of both values is same. Figure 14 compares the theoretical values by equation (8) and measured values of the low-speed mode. Although the both values in Fig. 14 are not similar, generation of the low-speed mode in the diffuser is proven by this analysis. The low-speed mode can be explained as instability of potential flow through the diffuser. This type of instability has been confirmed as rotating stall of a radial vaneless diffuser.

The values calculated from equation (9) are shown in Fig. 15 in the case in which α = 45º and λ =1. The low and high-speed modes are obtained according to the values r_1/ r_2 and r_2/ r_s. The low-speed mode appears when forced vortex region extends in a wide range on the hub. However, further evaluation of equation (9) is a future problem, because there is no information on the value r_1/ r_2.

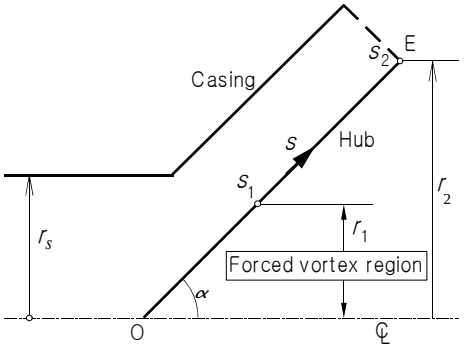

Fig. 13 Vaneless diffuser model for small perturbation analysis.

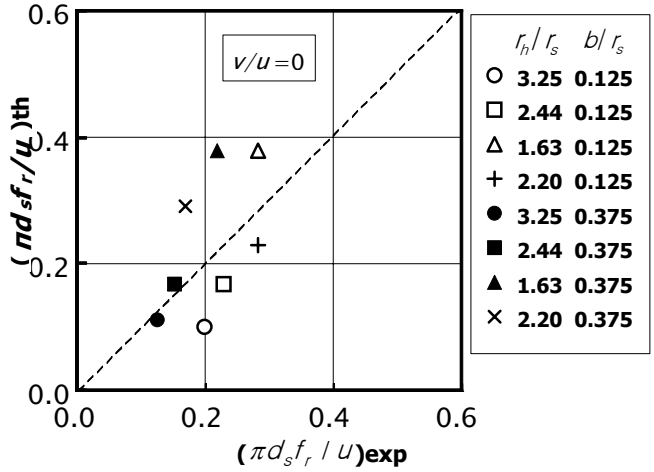

Fig. 14 Comparison of experimental and theoretical values by Eq. (8).

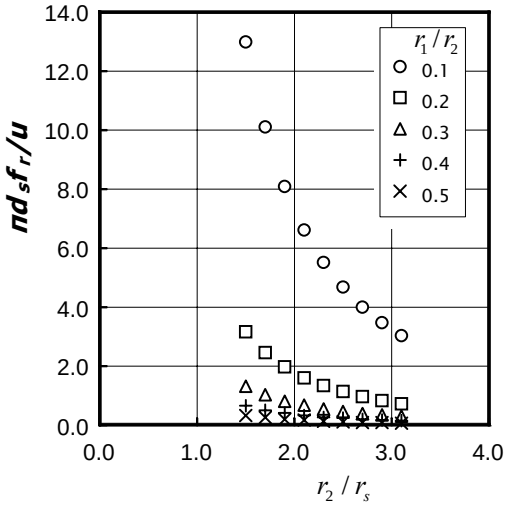

Fig. 15 Theoretical values of nondimensional rotational speed (Eq. (9), α=45°, v/u=0, λ=1).

4.4.2 Instability of Flow in Straight Tube (High-Speed Mode)

Under the assumption that the high-speed mode is associated with instability in the tube, two-dimensional analysis was carried out. The velocity components and pressure are assumed as follows.

$$v_r = \tilde{v}_r(r)e^{i(\lambda\theta-\omega t)} \tag{10}$$

$$v_\theta = v_0(r) + \tilde{v}_\theta(r)e^{i(\lambda\theta-\omega t)} \tag{11}$$

$$p = p_0(r) + \tilde{p}(r)e^{i(\lambda\theta-\omega t)} \tag{12}$$

The flow rate is assumed to be zero. For time-averaged flow, forced vortex motion at $0 \le r \le r_1$ and free vortex motion at $r_1 \le r \le r_s$ are assumed. The velocity components and pressures in two regions are continuous at $r = r_1$, respectively. Assumed boundary conditions are that perturbations of velocity components are definite at $r = 0$ and $v_r = 0$ at $r = r_s$. Upon solving linearized equations of motion, an angular velocity (eigenvalue) is obtained. The nondimensional rotational speed is obtained as shown in the following equation.

$$(\pi d_s f_r/u)_3 = (1/\lambda)(r_s/r_1)^2[(r_1/r_s)^{2\lambda} + \lambda - 1] \tag{13}$$

Similar analysis is presented in literature (Kurosaka [2]). In case where $\lambda = 1$, the value predicted from equation (13) is 1, irrespective of the value r_1/r_s. This value is close to the measured value for the high-speed mode. It is believed that the high-speed mode is due to instability of combined vortex flow in the tube.

5. Conclusion

The main findings of this study are as follows:

The experiment clarified that two kinds of unsteady flows, low and high-speed modes, were generated in the mixed-flow vaneless diffuser system. The critical value v/u for the onset of the low-speed mode is about 0.1.

The diffuser is the origin of the low-speed mode. The low-speed mode can be explained as instability of potential flow through the diffuser.

In the diffuser having a small radius ratio and a small cone angle, unsteady flow of the high-speed mode was generated. The high-speed mode is believed to result from instability of the combined vortex flow in the straight tube.

For the low-speed mode, an equation for nondimensional rotational speed at v/u=0 is presented. The applicable range is α = 22.5º ~ 45º, r_2/r_s = 1.6 ~ 3.2, and b/r_2 = 0.04 ~ 0.38.

Acknowledgments

The author wishes to thank Mr. Tsutomu Tagashira and Mr. Tomonari Oka, who are former graduate students of Fukuyama University, for their cooperation in the experiment.

Nomenclature

b	Diffuser width [m or mm]	v_s	Meridian velocity of the flow [m/s]
d_s	Inside diameter of the tube [m or mm]	v_θ	Peripheral velocity of the flow [m/s]
f	Frequency [Hz]	α	Cone angle of the hub [º]
f_r	Rotational speed of the cell [rps]	λ	Number of cells
l	Length of the tube [m or mm]	ρ	Fluid density [kg/m^3]
p	Pressure or pressure amplitude [Pa]	ω	Angular velocity [rad/s]
r	Radius [m or mm]		
r_e	Radius of the casing [m or mm]		Subscript
r_h	Radius of the hub [m or mm]	0	Steady component
r_s	Inside radius of the tube [m or mm]		
r_1	Radius of the forced vortex region [m or mm]		Superscript
r_2	Radius of the diffuser [m or mm]	$\sim$	Perturbation component
s	Meridian coordinate [m or mm]		
t	Time [s]		
u	Peripheral velocity of the inflow at $r = r_s$ [m/s]		
v	Averaged axial velocity of the flow [m/s]		
v_r	Radial velocity of the flow [m/s]		

References

[1] Escudier, M., 1987, “Confined Vortices in Flow Machinery“, Ann. Rev. Fluid Mech., 19, pp. 27-52.

[2] Kurosaka, M., 1982, “Acoustic Streaming in Swirling Flow and the Ranque-Hilsch (Vortex-Tube) Effect“, J. Fluid Mech., 124, pp. 139-172.

[3] Tsurusaki, H., et al., 1987, “A Study on the Rotating Stall in Vaneless diffusers of Centrifugal Fans“, JSME Int. J., 30(260), pp. 279-287.

[4] Nishi, M., et al., 1986, “Influence of Draft Tube Shape on the Characteristics of Pressure Surge and Flow Regime“, Trans. JSME, 52(481), pp. 3237-3243(in Japanese).

[5] Cassidy, J. J. and Falvey, H. T., 1970, “Observations of Unsteady Flow Arising after Vortex Breakdown“, J. Fluid Mech., 41(4), pp. 727-736.

[6] Tsurusaki, H. and Yokota, T., 2001, “Unsteady Flow Measured in a Mixed-Flow-Type Vaneless Diffuser System”, Trans. JSME, 67(654), pp. 398-403 (in Japanese).